Appendix I: Measurement of Surface Tension Using a Capillary Tube.

$\sigma = ?$

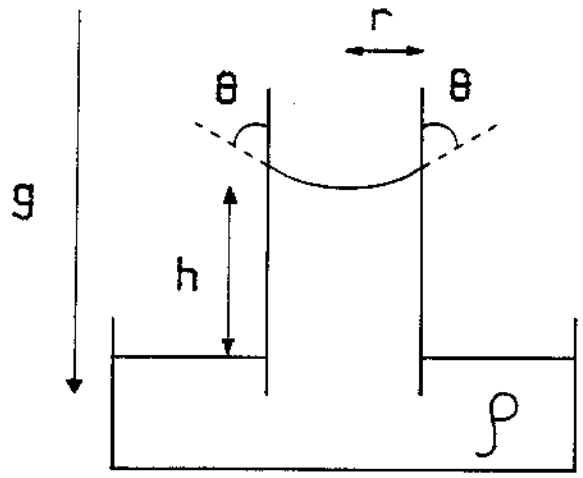


FIGURE: Liquid Rise in a Capillary Tube.

The height to which a liquid rises in a capillary tube is determined by the liquid's surface tension. Sears and Zemansky derive the following result:

$$\sigma = \frac{\rho g r h}{2\cos\theta}$$

The wetting agent Photo Flo reduces the contact angle to zero so:

$$\sigma = \frac{1}{2}\rho g r h$$

The pipettes used have a volume of 10 microliters between the black line and the far end. Measurement of this distance allows for calculation of the inner radius of the pipette.

# Surface tension restoring forces on gravity waves in narrow channels

David Heckerman, Steven Garrett,[a] and Gary A. Williams

*Physics Department, University of California, Los Angeles, California 90024*

Patrick Weidman

*Department of Aerospace Engineering, University of Southern California, Los Angeles, California 90007*
(Received 29 December 1978; final manuscript received 6 August 1979)

Surface tension restoring forces are investigated for low amplitude gravity waves propagating in narrow channels. Liquids which do not wet the container walls experience a nonuniform displacement of the meniscus as the wave passes. The variation of surface curvature leads to a surface tension force which increases the velocity of the gravity wave. The effect is substantial in experiments with water in Plexiglass channels. The dependence on channel width and contact angle has been investigated, and agreement is found with a simple theoretical model. Addition of a wetting agent to the water eliminates the effect, decreasing the velocity to within 1% of the classical dispersion relation.

## I. INTRODUCTION

In an infinitely wide channel the phase velocity of gravity-capillary waves propagating in a liquid of depth $h$, surface tension $\sigma$, and density $\rho$ is given by the well-known relation[1]

$$c^2 = (g/k + \sigma k/\rho)\tanh kh\,, \tag{1}$$

with $g$ the gravitational constant and $k = 2\pi/\lambda$ the wavenumber. However, in a narrow channel with bounding walls, the velocity can differ from this expression. An experiment by Walbridge and Woodward[2] with water in channels smaller than 1 cm in width gave velocities substantially higher than Eq. (1), and the velocities were found to be strongly dependent on the channel width. In an attempt to understand this phenomenon we have made a careful study of small amplitude wave propagation in narrow open channels. Our measurements provide evidence that the additional restoring force is a manifestation of variations in curvature of the fluid meniscus, and that contact angle hysteresis of the fluid at the channel walls plays an essential role. A simple model based on these features is in good agreement with the experimental data for channels wide compared with the capillary length.

Following a presentation of our preliminary results[3] we learned that Scott and Benjamin[4,5] have concurrently carried out an investigation of this same phenomena. Their variational formulation of the difficult Neumann boundary value problem gives rise to a Rayleigh quotient for estimating the frequency of wave propagation for a given wavelength. The choice of a quadratic spanwise profile for the oscillatory wave indeed furnishes an upper bound on the frequency in essential agreement with their careful experiments in brimfull channels. Our more intuitive (albeit inexact) development of the problem leads to a formula corroborating their results for relatively wide channels. Moreover, it has the advantage that it explicitly displays the effects of both channel width and fluid contact angle.

[a]Present address: Physics Department, University of California, Berkeley, Calif. 94720.

## II. APPARATUS

The gravity wave velocities were measured using a resonance technique in an annular channel, shown in Fig. 1. The waves generated with a plunger were detected by observing the mounding of the free surface with a capacitance gauge. As the frequency of the driving plunger was swept, resonances were observed at frequencies where an integral number of wavelengths fit into the mean circumference of the annulus, $n\lambda = 2\pi\bar{r}$, where $\bar{r}$ is the mean radius. (These frequencies differ by less than 1% from the exact Bessel function solutions for the channel dimensions used in the experiment.) A major advantage of the annular geometry is that there are no end effect corrections to the resonant frequencies.

After machining the channel out of Plexiglass stock, the test surfaces were polished smooth. A nominal channel depth of 2.0 cm was used throughout, and our initial 2.0 cm width had a mean circumference of 35 cm. In later experiments the channel width was varied between 1 and 3.5 cm. An aluminum top plate supporting the drive and detection systems covered the channel (see Fig. 1). Isolation of the resonator from ambient vibrations was effected by placing the channel on a heavy steel plate, which in turn rested on foam rubber pads.

The driving plunger was kept as small as possible to avoid perturbing the wave motion. It consisted of a no. 12 wire bent in an L shape, with the flat 1 cm length just underneath the liquid surface and aligned along the

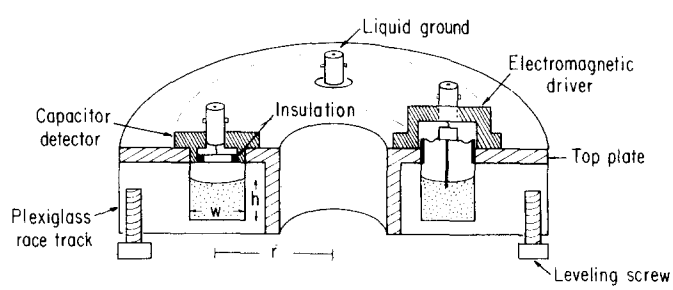


FIG. 1. Cross-sectional sketch of the annular resonator.

 0031-9171/79/122270-07$00.90  

channel. The other end of the wire was attached to the drive mechanism of a 5 cm loudspeaker from which the cone and cone support had been removed. Driving this 8 Ω loudspeaker with up to 1 V rms from an oscillator at frequencies between 1 and 10 Hz generated gravity waves with mounding amplitudes as large as $10^{-2}$ cm.

Opposite the driver, a 2 cm diam capacitance plate was mounted flush with the top cover using epoxy resin for insulation. The liquid constituted the second plate of the capacitor and hence was made conducting. Electrical contact was made by immersing the tip of a coaxial connector in the liquid. With the fluid level 3 mm below the cover plate, a capacitance of about 1 pF was detected by the capacitance gauge.

The operating sequence of the driving and data acquisition electronics illustrated schematically in Fig. 2 is as follows: A voltage controlled oscillator is slowly swept over the range 1–10 Hz using an external ramp voltage. The oscillator drives a power amplifier which in turn drives the plunger. The motion of the surface at the detector plate then causes oscillations in the capacitance which are detected as the off-null signal from a General Radio 1615A capacitance bridge. The bridge is operated with a 5 kHz, 30 V p-p oscillator that also serves as the reference for a lock-in amplifier (Princeton Applied Research model 129A). The output voltage of the lock-in (which oscillates at the 1–10 Hz drive frequency) is rectified and filtered with a very low frequency ac to dc converter, and is plotted versus frequency on an $x$-$y$ recorder. The sensitivity of the system is quite high; mounding amplitudes as small as $10^{-4}$ cm were readily observed.

A typical frequency sweep is shown in Fig. 3. Because of the low frequencies involved, it was imperative, in taking the measurements, to sweep very slowly, allowing at least 60 min for a complete sweep over the 1–10 Hz range. The recorded peaks were sharp enough so that the resonant frequencies (and hence the velocities) could be determined to within about 1%. The observed quality factors of the resonances were fairly close to those expected theoretically taking into account viscous losses at the walls[1] and also the surface attenuation.[6]

A second, and faster, technique for measuring the resonant frequency of the fundamental mode is to time the free decay oscillations of the system. Tapping the

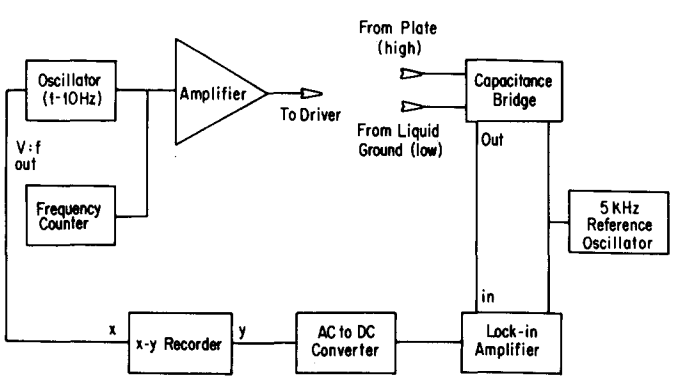


FIG. 2. Block diagram of the electronics.

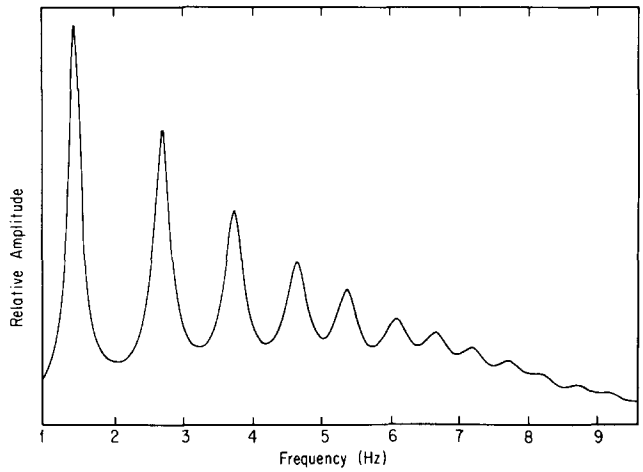


FIG. 3. A typical spectrum from the resonator using water.

resonator very lightly primarily excites the fundamental mode, and the frequency of the oscillations can then be measured directly with a frequency counter (in the period mode) or by plotting the signal on a chart recorder with a calibrated time base. Frequencies measured in this way agreed to within 1% of those found with the swept resonance technique.

## III. INITIAL RESULTS

Initial experiments were carried out with this system using distilled water to which a few mg of NaCl was added to make it conducting (the salt does not appreciably affect the surface tension or viscosity of water[7]). The results for the velocity dispersion are shown as the circular data points in Fig. 4. As is readily apparent the velocities are consistently about 13% higher than Eq. (1) (the solid line). However, the points do display the correct functional form of the dispersion expected. The data points for water fit very well to an expression of the form

$$c^2 = [(g + \Delta g)/k] \tanh kh \,, \tag{2}$$

where $\Delta g$, an additional restoring acceleration, is found to have the value $\Delta g/g = 0.28 \pm 0.01$ (the term $\sigma k/\rho$ is negligible at these low frequencies).

Inspection of the water in the channel showed that it did not wet the Plexiglass. Furthermore, we observed that the contact line repeatedly grabbed at and broke away from the channel walls while the resonator cavity was slowly being filled. The tendency for nonwetting liquids to "lock" at a wall is a well-known phenomenon.[8] To investigate whether this effect was influencing the gravity wave velocities, a wetting agent (about 0.5 cc of Kodak Photoflo 200) was added to the water; measurements for this case are shown as the squares in Fig. 4. Agreement with Eq. (1) is found to within 1%, suggesting that the lack of wetting at the channel walls is responsible for the higher velocities found in the water.

## IV. MODEL CALCULATION

Based on the results of the previous section, a model for the extra restoring force can be formulated by making the assumption that a liquid which does not wet the

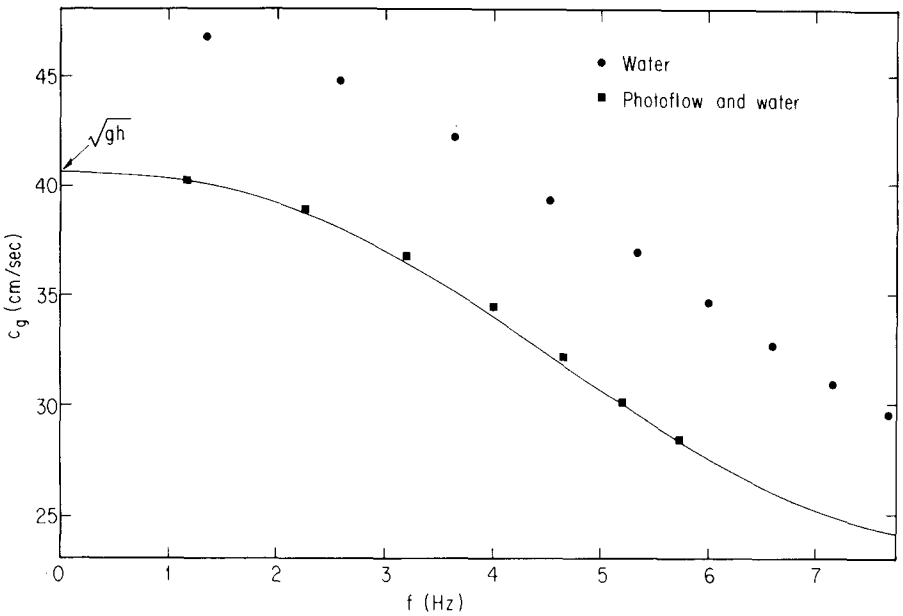


FIG. 4. Velocity dispersion for water (circles) and water with Photoflo (squares). The solid line is Eq. (1).

channel wall is locked in place there. In such a situation a gravity wave will experience a nonuniform displacement of the meniscus as the wave passes, the displacement falling to zero at the walls. The resulting change in the curvature of the surface will lead to surface tension restoring forces. The assumption of locking at the wall, certainly not valid for large amplitude waves, is reasonable for the range of wave amplitudes ($10^{-4}$–$10^{-2}$ cm) encountered in the present experiment. The zero displacement of the wave at the channel walls is visually observed in this apparatus, and is also reported in Refs. 2, 4, and 5.

Figure 5 shows a schematic of the geometry employed. Choosing $x$, $y$, and $z$ to be the down channel, cross channel, and vertical coordinates, respectively, the displacement $\xi$ of the surface from the equilibrium meniscus profile $\zeta(y)$ can be written

$$\xi(x, y, t) = z(x, y, t) - \zeta(y) = \xi_0(x, t)\eta(y)\,, \tag{3}$$

where $\eta(0) = 1$ and $\eta(\pm\frac{1}{2}w) = 0$, with $w$ the width of the channel. The extra pressure resulting from the change in surface curvature is given by the formula of Young and Laplace

$$\Delta p = \sigma[K(\zeta + \xi) - K(\zeta)]\,, \tag{4}$$

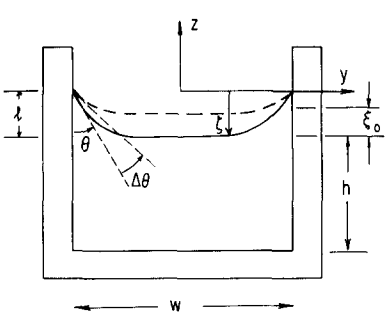


FIG. 5. Geometry used in the model calculation. The propagation direction of the gravity wave is the $x$ axis out of the page. The quantities $\xi_0$ and $\Delta\theta$ are exaggerated for the purpose of illustration.

where $K(z)$ is the compound curvature given by

$$K(z) = \frac{(1 + z_x^2)z_{yy} - 2z_x z_y z_{xy} + (1 + z_y^2)z_{xx}}{(1 + z_x^2 + z_y^2)^{3/2}}\,, \tag{5}$$

and the subscripts denote partial differentiation with respect to the variable. We shall consider only linear waves for which the horizontal gradients of $\xi$ are everywhere small. Then, Eq. (4) gives

$$\Delta p = \sigma\left[\frac{\partial}{\partial y}\left(\frac{\xi_y}{(1 + \zeta_y^2)^{3/2}}\right) + \frac{\xi_{xx}}{(1 + \zeta_y^2)^{1/2}}\right] \tag{6}$$

to first order in the small quantities. We note that a nonplanar equilibrium surface affects both the cross channel and down channel curvature terms; when the equilibrium surface is flat, the term in brackets is simply the horizontal Laplacian of $\xi$. We further restrict the analysis to long waves as realized in our experiments, and in this case the down channel curvature term in (6) can be neglected.

To study wave propagation, we assume that the channel is wide enough so that it is possible to use a velocity potential to describe the flow. This will be valid for channels much wider than the viscous penetration depth $\delta = (2\nu/\omega)^{1/2}$, where $\nu$ is the kinematic viscosity and $\omega$ is the angular frequency. ($\delta = 0.6$ mm for water at a frequency $f = \omega/2\pi = 1$ Hz.) Also, for a wide channel, $\eta$ will be close to unity except for the regions within a capillary constant $a = (2\sigma/\rho g)^{1/2}$ (= 3.9 mm for water) from the walls. The validity of this assumption can only be ascertained *a posteriori* by comparing predicted results with experiment, but it is consistent with the use of the potential function for waves in an unbounded channel[1]

$$\phi = A \cosh k(z + h) \exp[i(kx - \omega t)] \tag{7}$$

as the approximate potential function for our problem. The boundary condition determining the dispersion of the gravity waves, that the pressure in the liquid at the free surface equal the ambient pressure, must now be altered to include the surface tension pressure given by Eq. (6). Averaging the free surface boundary condition[1]

across the width of the channel for a $y$-independent velocity potential gives

$$\frac{\partial^2\phi}{\partial t^2} = \left(-g + \frac{\overline{\Delta p}}{\rho}\right)\frac{\partial\phi}{\partial x} \tag{8}$$

where $\overline{\Delta p}$ is the average surface tension pressure,

$$\overline{\Delta p} = \frac{1}{w}\int_{-w/2}^{w/2} \Delta p \; dy = \frac{2\sigma}{w}\xi_0 \sin^3\theta \left.\frac{d\eta}{dy}\right|_{w/2} \tag{9}$$

with $\theta$ the liquid-solid contact angle. The velocity potential in Eq. (7) then yields a dispersion relation of the form given by Eq. (2) with the augmented acceleration

$$\Delta g = -\frac{2\sigma}{\rho w}\sin^3\theta \left.\frac{d\eta}{dy}\right|_{w/2}. \tag{10}$$

The derivative of $\eta$ at the channel wall can be written in terms of the change in the contact angle, $\Delta\theta$, which occurs when the liquid level changes. From the geometry of Fig. 5, the change in slope of the surface at $y = \frac{1}{2}w$ as a wave of amplitude $\xi_0$ passes is given by

$$[\cot(\theta + \Delta\theta) - \cot\theta] = -\Delta\theta/\sin^2\theta \tag{11}$$

and from Eq. (3) we obtain

$$\left.\frac{d\eta}{dy}\right|_{w/2} = -\Delta\theta/\xi_0 \sin^2\theta\,. \tag{12}$$

In accordance with the wide channel approximation, $w \gg a$, the height to which the meniscus rises at the wall is related to the contact angle by

$$l = \begin{cases} +a(1-\sin\theta)^{1/2}, & \theta \leq \frac{1}{2}\pi\,, \quad (13a) \\ -a(1-\sin\theta)^{1/2}, & \theta \geq \frac{1}{2}\pi\,. \quad (13b) \end{cases}$$

With our assumption of complete locking at the wall, the change in contact angle is then related to the displacement by

$$a(1-\sin\theta)^{1/2} - \xi_0 = a[1 - \sin(\theta + \Delta\theta)]^{1/2} \quad (\theta < \tfrac{1}{2}\pi) \tag{14}$$

or, expanding for small $\Delta\theta/\theta$,

$$\frac{\Delta\theta}{\xi_0} = \frac{2(1-\sin\theta)^{1/2}}{a\cos\theta}\,. \tag{15}$$

Substituting this into Eqs. (10) and (12) gives the final expression for the fractional increase in acceleration

$$\Delta g/g = (1/D)\,|\tan\theta|\,(1-\sin\theta)^{1/2} \quad (D \gg 1)\,, \tag{16}$$

where $D = w/2a$ is the nondimensional channel width, and the absolute value sign stems from a similar analysis for $\theta > \frac{1}{2}\pi$. For sufficiently wide channels, our model shows that the additional acceleration is inversely proportional to the channel breadth. We also note that the spanwise curvature has its greatest effect when $\theta = 90°$, in which case the fractional acceleration is given by

$$\lim_{\theta\to\pi/2}(\Delta g/g) = 1/\sqrt{2}D\,. \tag{17}$$

To compare this to the experimental $\Delta g$ for water the contact angle with Plexiglass is needed. This was measured by tilting the resonator and finding the tilt angle at which the meniscus at the wall becomes perfectly level. The (advancing) contact angle was found to be $83° \pm 3°$. The advancing angle is used because the channel is filled slowly, with no sloshing, leaving the meniscus at the advancing angle. Substituting this into Eq. (16) and using $\sigma = 72$ dyn/cm for water (checked by a capillary rise technique) gives, for the 2 cm channel, $\Delta g/g = 0.27 \pm 0.01$, in good agreement with the observed value $\Delta g/g = 0.28 \pm 0.01$.

## V. FURTHER MEASUREMENTS

In this section we present the results of experiments designed to test the functional dependence of the extra acceleration on both channel width $D$ and contact angle $\theta$.

### A. The effect of channel width

Measurements of the fundamental resonance frequency for waves in channels both wider and narrower than the original 2 cm were performed and these data are plotted in Fig. 6. We have used Eq. (2) including the classical capillary term $\sigma k/\rho$ to present the measurements of Walbridge and Woodward[2] and also those of Benjamin and Scott[5]. From Eq. (6) we see that this capillary term remains unaltered in the cross channel average only when the static meniscus profile is exactly horizontal; this is true in the experiments of Benjamin and Scott,[5] and the effect of $\zeta_y$ is negligible for the inferred 83° contact angle in the experiments of Walbridge and Woodward.[2] In a private communication with Woodward, we learned that the material used for their channel walls was Plexiglass; this was not reported in Ref. 2. Hence, we assume their contact angle was about 83° as in the present experiment. They used clean water, but observed that the meniscus was irregular at the edges and had poor reproducibility of their data from day to day. Benjamin and Scott used clean water between straight Perspex walls and forced the contact angle to be 90° (but see paragraph 1, Sec. VB) by filling their channels to the brim. We have averaged their 15 or so separate measurements taken at varying wavelengths in each of three channels and found quite constant values of $\Delta g/g$. The averaged values are 5.36 $\pm 0.11$, $0.820 \pm 0.058$, and $0.294 \pm 0.021$ for nondimensional widths $D = 0.522$, 1.38, and 2.65, respectively.

The solid line in Fig. 6 is a plot of Eq. (16) for $\theta = 83°$, although the difference between this and 90° is not dis-

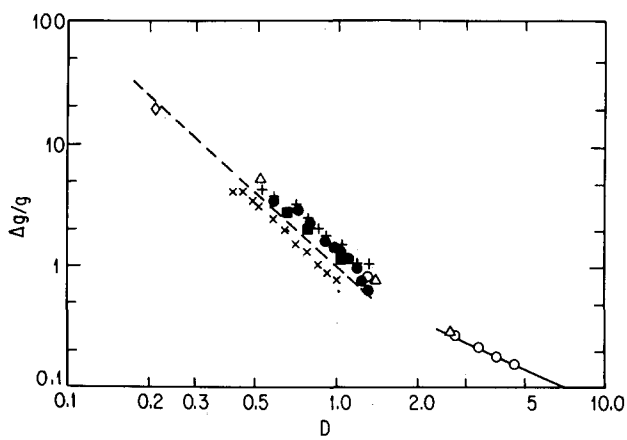


FIG. 6. Dependence of $\Delta g/g$ on channel width: ○ present measurements; + ● × ■ 20 Hz data, ◇ 60 Hz data of Walbridge and Woodward[2]; △ averaged data points of Benjamin and Scott[5]; —— Eq. (16), ---- Eq. (A3), both evaluated at $\theta = 83°$.

cernible on the log-log scale. The plotted data confirm the $1/D$ dependence for sufficiently wide channels, i.e., $D \gtrsim 2.5$ for contact angles near 90°. The deviation from (16) for narrower channels is to be expected because a number of assumptions used in its derivation are no longer valid as the channel width becomes of the order of a few capillary lengths. Equation (13) in particular becomes a poor approximation as the surface begins to resemble a circular arc.

The experimental data corresponding to the narrower channels suggest a $1/D^2$ dependence and, in fact, the upper bound equation for narrow channels cited by Scott and Benjamin[4,5] exhibits this result. In Appendix A we present a simple geometrical argument to explain the inferred narrow channel behavior. This approximate relation given by Eq. (A3), valid for $D \ll 1$, is plotted for $\theta = 83°$ as the dashed line in Fig. 6.

### B. The effect of contact angle

A variation in the limiting macroscopic angle of the fluid at the walls can be obtained by overfilling a channel. In this situation the fluid is observed to remain pinned at the inner and outer corners until some overfill volume $\Delta V$ (the actual volume less the volume of a channel filled flat to the top) is exceeded. Although surface chemists may generally regard the microscopic contact angle as an invariant for a given solid-liquid-gas interface, Lomas[9] has shown that for an inclined drop the solution to Young's equation leads to different leading and trailing contact angles. Thus, both the inclined drop and overfilled channel show that the macroscopic contact angle is indeed affected by the geometry of the system as a consequence of gravitational effects. We shall not attempt to differentiate between true (microscopic) and observed (macroscopic) contact angles in what follows.

As suggested here, we have chosen to simulate a variety of contact angles by overfilling two channels which satisfy the wide channel criterion $D \gtrsim 2.5$. Because of the annular geometry, the inner and outer contact angles will be different. The analysis and observations reported in Appendix B suggest that these angles for our 2 and 3.5 cm channels always differed by less than two degrees, and hence we use the average contact angle $\bar{\theta} = \frac{1}{2}(\theta_1 + \theta_2)$ ($\theta_1$ and $\theta_2$ are the inner and outer contact angles, respectively) to present our results. Furthermore, the analysis in Appendix B shows that an annular channel cannot support an outer contact angle of 180°, the maximum theoretical values being 168.6° and 167.8° for the 2 and 3.5 cm channels, respectively.

The measured values (open symbols) of $\Delta g/g$ from the overfill experiments are presented in Fig. 7. The solid curves were determined from Eq. (16), the dashed curves are an aid to display the experimental trends, and the error bars are indicative of the reproducibility of the measurements. The displaced data point for the 3.5 cm channel near $\bar{\theta} = 155°$ is probably due to measurement error.

As expected, the additional acceleration decreases away from $\bar{\theta} = 90°$, although the fall off of the measured

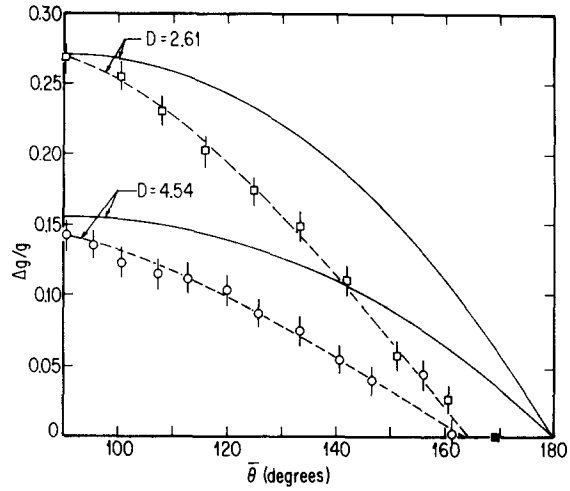


FIG. 7. Dependence of $\Delta g/g$ on contact angle: ϕ measurements for $D = 4.54$, ⊕ measurements for $D = 2.61$; ---- trends of experimental data used to find zero $\Delta g$ values of $\bar{\theta}$; —— Eq. (16) evaluated using $\bar{\theta}$; ■ maximum values of $\bar{\theta}$ from the numerical results given in Appendix B.

values is substantially greater than that given by the two-dimensional model. Even though such a large discrepancy was not anticipated, the measurements are consistent with the results in Appendix B, i.e., probably the effect of cross-channel surface tension on the wave speed disappears when the overfill volume reaches its maximum value corresponding to $\bar{\theta}_{max} = 169.5°$ and 169.2° for the 2 and 3.5 cm channels, respectively. These values are plotted as the solid squares in Fig. 7. An extrapolation of the experimental data (neglecting the single faulty measurement point) to $\Delta g = 0$ gives $\bar{\theta} \approx 164°$ for both channels, close to that actually estimated at breaking ($\bar{\theta} \approx 166°$) from our observation in the 3.5 cm channel.

## VI. SUMMARY AND CONCLUSION

That free surface gravity waves in narrow channels can propagate significantly faster than waves in an unbounded medium is now well established. The present work corroborates the analysis by Benjamin and Scott[5] in showing that these larger phase speeds are due to the change in surface curvature induced by a passing wave when the fluid contact line remains fixed at the walls. The original measurements of Walbridge and Woodward[2] show that the effect can be substantial: for water in a 1.7 mm channel, a restoring force almost 20 times that of gravity is observed.

Our theoretical model for channels wide compared with the capillary length is in good agreement with experimental data for $D \gtrsim 2.5$ when the contact angle is near 90°. The overfill experiments performed to simulate a variety of contact angles do not give direct confirmation of the $\theta$ dependence predicted by the two-dimensional model. However, the analysis in Appendix B suggests that the observed deviations are due solely to the annular geometry of our test facility and, therefore, we have no reason to doubt that Eq. (16) can be used to correctly determine the effect of contact angle for relatively wide, straight channels.

When the channel width is comparable to or smaller than the capillary length, accurate upper bounds on the phase speeds can be obtained from the Rayleigh quotient given by Benjamin and Scott[5] when the fluid surface is horizontal, and they show how their analysis may be extended to include nonplanar surfaces. Our simple result given in Appendix A apparently gives the correct asymptotic (in the limit $D \to 0$) $1/D^2$ trend, but with smaller magnitude than found in Refs. 4 and 5.

In closing we note that this phenomenon may be of practical interest to surface chemists. Whereas fluid dynamicists are generally more interested in determining the fluid motion resulting from the observed contact angle hysteresis, detection of the increased wave speed may, in fact, prove to be a useful means of investigating the wetting properties of fluids at solid surfaces.

## ACKNOWLEDGMENTS

We would like to thank I. Rudnick for many useful discussions concerning this project, and also S. Adams and J. Marcus for help in constructing and operating the apparatus.

This work was supported by University of California funds for instructional equipment, and by the National Science Foundation, Contract DMR 78-2008, and by the Office of Naval Research, Contract N00014-75-C-0246. One of us (G.A.W.) would like to acknowledge receipt of an Alfred P. Sloan Research Fellowship.

## APPENDIX A

The meniscus profile for fluid contained between closely spaced parallel vertical walls takes the form of a circular arc. With the fluid pinned at the walls, we assume that a small wave of amplitude $\xi_0$ will simply alter the arc radius to accommodate the change in volume. From the geometry in Fig. 8, one obtains

$$H = (w/2)[(1 - \sin\theta)/\cos\theta], \tag{A1}$$

and hence the narrow channel counterpart of Eq. (15) is

$$\frac{\Delta\theta}{\xi_0} = -\frac{d\theta}{dH} = \frac{2}{w}\frac{\cos^2\theta}{(1-\sin\theta)}. \tag{A2}$$

Combining this result with Eqs. (10) and (12) gives the desired result

$$\frac{\Delta g}{g} = \frac{1}{2D^2}\frac{\sin\theta\cos^2\theta}{(1-\sin\theta)} \quad (D \ll 1). \tag{A3}$$

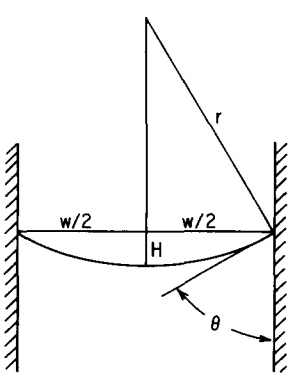


FIG. 8. Geometry of meniscus profile for very narrow channels.

This equation is plotted as the dashed line in Fig. 6 for the experimental value $\theta = 83°$. The maximum value at $\theta = 90°$ is given by

$$\lim_{\theta \to \pi/2} (\Delta g/g) = 1/D^2. \tag{A4}$$

Although this result is quite simple, it is certainly not exact. The use of the $y$-independent velocity potential of Eq. (8) is no longer a good approximation for the narrow channel case. The amplitude $\xi$ of the wave will vary continuously across the channel, and this factor is taken into account in the theoretical calculations of Benjamin and Scott.[4,5]

## APPENDIX B

The annular geometry of our test facility necessarily gives rise to a compound curvature in the equilibrium meniscus shape, the effects of which increase with decreasing radius. In order to assess the importance of this three-dimensional behavior on the macroscopic contact angle at the inner and outer walls, we solve the equation of Young and Laplace

$$z_{rr} = (1 + z_r^2)^{3/2}(2z/a^2 - 1/r) \tag{B1}$$

describing the balance between surface tension and hydrostatic force for fluid contained in an annular channel. Here, $z$ is the vertical surface coordinate, $r$ is the radius, $1/r$ is the additional curvature, and the signs chosen correspond to $\frac{1}{2}\pi \leq \theta \leq \pi$. The boundary conditions appropriate for the overfill experiment in Sec. VB are

$$\frac{dz}{dr} = \cot\theta_1 \quad \text{at } r = r_1, \tag{B2}$$

$$z = z_0 \quad \text{at } r = r_1 \text{ and } r = r_2. \tag{B3}$$

The actual overfill profile is given by $\zeta(r) = z(r) - z_0$. Solutions are obtained by iteration on $z_0$ until (B3) is satisfied for a given choice of $\theta_1$ in (B2). Equation (13b) provides a reasonable first guess for $z_0$ when the inner

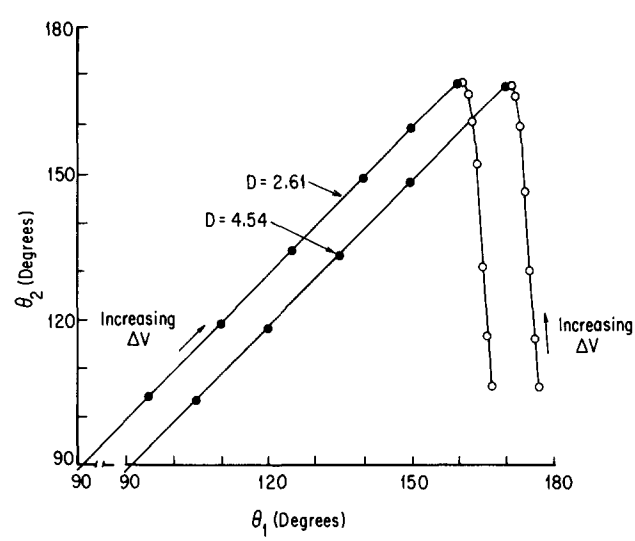


FIG. 9. Relation between outer ($\theta_2$) and inner ($\theta_1$) contact angles for the wide ($r_1 = 4.460$ cm, $r_2 = 7.940$ cm) and narrow ($r_1 = 4.725$ cm, $r_2 = 6.725$ cm) channels. Numerical results for the left branch (almost symmetric meniscus profiles) are given by the dots; results for the right branch (asymmetric meniscus profiles) are given by the open circles.

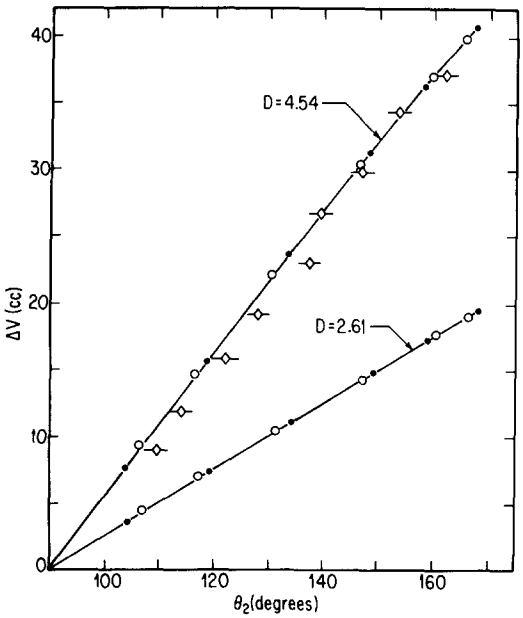


FIG. 10. Variation of overfill volume with outer contact angles for the two channels using the same symbols for the left and right branch solutions described in Fig. 9;-◇- experimental data for the wide (3.5 cm) channel.

radius $r_1$ is sufficiently large. The two-point boundary value problem is sensitive in that very accurate values of $z_0$ are required to attain convergence for long integration paths. Success was obtained with double precision for the 2 and 3.5 cm channels, but wider channels would have necessitated more sophisticated integration techniques, such as the shooting-splitting method described by Firnett and Troesch.[10]

Surprisingly, the numerical computations yield two solution curves for a given overfill volume $\Delta V$ as indicated in Fig. 9. The left branch (solid dots) shows that the outer angle $\theta_2$ increases at nearly the same rate as the inner angle $\theta_1$, although $\theta_2$ is always less than $\theta_1$ for both channels; the meniscus profiles (not shown) are quite symmetric and relatively flat in the midchannel region. The right branch (small open circles) bends over steeply near $\theta_1 = 170°$ and could not be continued beyond $\theta_1 = 177°$ owing to the extremely sensitive behavior of the integrations in this region. These latter solutions appear physically unacceptable in that a substantial asymmetry in the meniscus profile develops as $\theta_2$ decreases from its maximum value.

In Fig. 10 we show the variation in overfill volume as a function of $\theta_2$ using the same symbols as in Fig. 9. Note that the results for both solution branches practically fall along a common curve. Measurements of the outer limiting angle for the 3.5 cm channel were made with a comparator microscope fitted with a goniometer and focused on the surface profile at the outer edge. The overfill volumes were determined by weighing (to the nearest 0.02 g) each added increment of fluid. The results are plotted in Fig. 10 with an estimated error bar of $\pm 2°$. Similar measurements for the narrower channel were not obtained because the microscope could not be located close enough to the edge to obtain a sharp focus.

It was clear from visual observations that the overfilling of the channel proceeded along the left branch in Fig. 9. For example, a sighting across the approximately level surface corresponding to $\Delta V \approx 0$ showed that the inner portion of the surface at $r_1$ was inclined 1 or 2 deg while the outer portion near $r_2$ was essentially flat. The contact line at the inner wall broke with the addition of fluid beyond the last measured value; we estimate $\theta_2 \approx 165°$ at the breaking point, somewhat less than the maximum value ($\theta_2 = 167.8°$) suggested by our numerical results.

The apparent agreement between experiment and prediction in Fig. 10 is our basis for using the theoretical curves to determine the average contact angle. The accuracy in determining the incremental volume is clearly superior to that of measuring the contact angle. Having measured the overfill volume, $\theta_2$ is obtained from Fig. 10 and then $\theta_1$ is determined from Fig. 9; the contact angle $\bar{\theta}$ used in Sec. VB is simply the arithmetic mean of these two values. From the results in Fig. 9 the estimated value of $\bar{\theta}$ at breaking for the 3.5 cm channel is 166°.


[1]L. D. Landau and E. M. Lifshitz, *Fluid Mechanics* (Pergamon, London, 1959).

[2]N. L. Walbridge and L. A. Woodward, Phys. Fluids **13**, 2461 (1970).

[3]D. Heckerman, S. Garrett, and G. Williams, Bull. Am. Phys. Soc. **23**, 996 (1978); D. Heckerman, *ibid.* **24**, 37 (1979).

[4]J. C. Scott and T. B. Benjamin, Nature **276**, 803 (1978).

[5]T. B. Benjamin and J. C. Scott, J. Fluid Mech. **92**, 241 (1979).

[6]F. C. Goodrich, Proc. Roy. Soc. London Ser. A **260**, 490 (1961).

[7]*Handbook of Chemistry and Physics* (Chemical Rubber, Cleveland, Ohio, 1962), 44th ed., p. 1234.

[8]N. K. Adam, *The Physics and Chemistry of Surfaces* (Dover, New York, 1968), p. 180.

[9]H. Lomas, J. Coll. Interface Sci. **33**, 548 (1970).

[10]P. J. Firnett and B. A. Troesch, *Lecture Notes in Mathematics* (Springer-Verlag, Berlin, 1974), Vol. 362, p. 408.

# Observation of a Nonpropagating Hydrodynamic Soliton

Junru Wu, Robert Keolian, and Isadore Rudnick
*Department of Physics, University of California, Los Angeles, California 90024*
(Received 30 January 1984)

When a trough resonator partially filled with water is parametrically driven at an appropriate frequency and amplitude, one or more surface-wave solitons with polaronlike behavior are created. Their properties and interactions are described.

PACS numbers: 47.35+i

We report on the experimental discovery of a nonpropagating hydrodynamic soliton, and describe its properties including the interaction between solitons. It is a surface wave in water contained in a trough resonator undergoing continuous excitation.

The apparatus is quite simple. We use a Plexiglas channel 38 cm long and 2.54 cm wide filled with water to a depth of 2 cm. Several drops of the wetting agent Kodak Photo-Flo are added to minimize surface pinning at the walls. Waves are generated by placing the horizontal trough on a loudspeaker whose cone is driven at a frequency $2\nu$ of about 10 Hz in the vertical direction. Below a certain threshold there is little or no significant wave generation. Above the threshold there is a parametrically excited wave[1,2] at half the drive frequency.

Suppose the trough were very long so that it can be regarded as a waveguide with width coordinate $y$ and length coordinate $x$. The depth $h$ controls the gravity wave phase velocity $c$ given by[3]

$$c^2 = (g/k)\tanh(kh). \tag{1}$$

The surface height is given by[4]

$$z = z_0 \cos(k_y y)\exp[i(k_x x \pm 2\pi\nu t)] \tag{2}$$

where $k_y l_y = q\pi$, $l_y$ is the width, $q = 1, 2, 3, \ldots$, and

$$k^2 = k_x^2 + k_y^2 = (2\pi\nu)^2/c^2. \tag{3}$$

The case $q = 0$ is the plane-wave mode, $q = 1$ has one velocity antinode between the side walls, $q = 2$ has 2, etc. If $\nu < \nu_{\text{cutoff}} = qc/2l_y$ then $k_x$ is imaginary, the amplitude down the waveguide decays exponentially, and energy will not propagate, but is instead reflected back. For a finite waveguide of length $l_x$,

$$z = z_0 \cos(k_x x)\cos(k_y y)\cos(2\pi\nu t)$$

where $k_x l_x = p\pi$ and $p = 0, 1, 2, 3, \ldots$ . Resonances are given by

$$\nu_{p,q} = \frac{c}{2}\left[\left(\frac{p}{l_x}\right)^2 + \left(\frac{q}{l_y}\right)^2\right]^{1/2}. \tag{4}$$

The $(p,q) = (0,1)$ mode is the equivalent of being at the first cutoff for the infinite waveguide.

We find that we can observe all the low-lying $(p,0)$ modes with the parametric drive. If instead of the vertical parametric excitation we excite the resonator by oscillating it horizontally in the $y$ direction, we find that $\nu_{0,1}$ is a function of the response amplitude, being lower the higher the amplitude. It decreases by 20% when the peak height increases from a very small value to 2 cm. When we parametrically excite the (0,1) mode, however, it appears to be unstable.

What we observe instead of the (0,1) mode are one or more excitations highly localized in the $x$ direction, "sloshing" in the $y$ direction. It is suprising and intriguing that while all parts of the trough are oscillated with equal amplitude, the vigorous wave motion occurs in a space of only a few centimeters long while the rest of the water remains quiet. The phase shift along $x$ given by Eq. (2) for $\nu_{\text{cutoff}} = 5.1$ Hz and $\nu = 5.4$ Hz is 90° in a distance of 6 cm. Yet, within our resolution of 3°, we find no measurable phase difference between any two points in the wave. We believe that this absence of a phase difference is of fundamental importance; the wave is not simply a waveguide mode occurring slightly above the cutoff frequency but a new type of nonpropagating solitary wave. As we continue we shall see that it has properties usually associated with solitons and shall, accordingly, use this term in describing its behavior. Figure 1 is a computer-generated profile of the soliton based on measurements taken from photographs, when it is at its peak on the far side of the trough. Half a period later the wave peak will have the same height on the near side of the trough. The wave frequency here is 5.1 Hz.

Essentially identical phenomena have been observed in an annular resonator 72 cm in mean circumference and 2.2 cm wide, and in a straight resonator 19 cm long. With a horizontal drive on a linear resonator we have also seen the soliton, accompanied, however, by a low-amplitude (0,1)

 

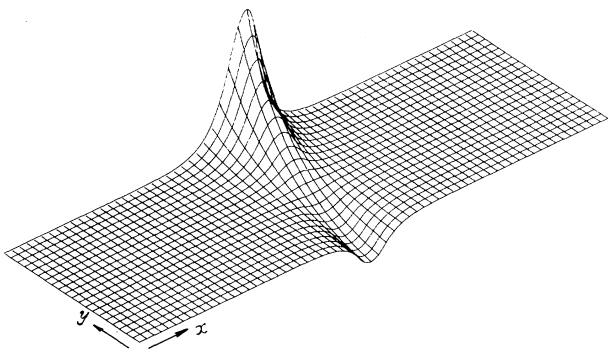


FIG. 1. A plot of

$$z = \mathrm{sech}(x/1.12)[2.8\exp(-1.1y) - 0.70] \times \cos(2\pi \times 5.1t)\ \mathrm{cm},$$

at $t = 0$, which is a profile of the soliton based on curve fits to measurements taken from photographs.

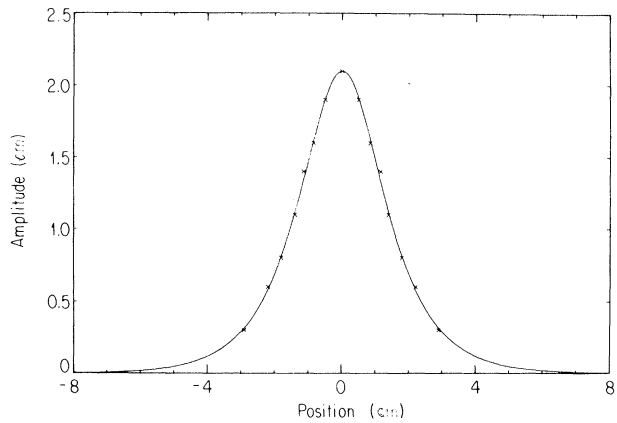


FIG. 2. The height of the soliton as a function of $x$. The points are experimental data, and the solid curve is $z = 2.1\,\mathrm{sech}(x/1.12)$ cm.

mode. All this suggests that neither the parametric drive nor the resonator ends are central to understanding the phenomena.

We understand the localization of the soliton as the soliton "digging its own hole." Because $\nu_{\mathrm{cutoff}} = \nu_{0,1}$ is depressed at higher amplitudes, $\nu > \nu_{\mathrm{cutoff}}$ in the center of the soliton but $\nu < \nu_{\mathrm{cutoff}}$ in the wings. Energy cannot escape from the center; it is reflected back at its evanescent wings. This self-trapping is reminiscent of polaron behavior. Dr. L. A. Turkevich called the soliton a hydrodynamic polaron. We have also trapped solitons by placing a mound on the bottom of the trough so that there is a localized shallow.

Figure 2 is a plot of the height $z$ of the soliton as a function of $x$. The points are experimental and the curve is $z = 2.1\,\mathrm{sech}(x/1.12)$ cm, a functional dependence which characterizes some solitions.[5] At the tail of the hyperbolic secant the decay length, 1.12 cm, is equal to the low-amplitude waveguide evanescence length $\gamma$, and this is just the magnitude of $k_x^{-1}$. Thus we can determine the phase velocity of this wave from

$$c = \frac{\omega}{(k_y^2 + k_x^2)^{1/2}} = \frac{2\pi(5.1)}{[(\pi/l_y)^2 - 1/\gamma^2]^{1/2}} = 37.7\ \mathrm{cm/sec}.$$

Using Eq. (1) with a correction for surface tension[3] we find the value 33.7 cm/sec.

The dependence of $z$ on $y$ when the wave is at its peak was found to be far from a cosine function. A best-fit curve is $z = 2.8\exp(-1.1y) - 0.70$ cm.

If we slightly tilt the trough the soliton slowly moves toward the shallow end. For a slope of 0.05, for instance, the soliton's average speed is 0.05 cm/sec. When the trough and loudspeaker are accurately horizontal the soliton maintains its $x$ position in the trough for times the order of an hour or more. We hypothesize that this stability is due to pinning effects at the walls.

There is generally some degree of competition between the various modes of the trough. We have devised ways to selectively encourage the appearance of the solitons to the exclusion of competitive modes. One obvious way is to choose trough dimensions which separate in frequency the unwanted modes from the soliton mode. Another very successful procedure is to nucleate the soliton mode by producing a disturbance which is compatible with it. Thus sloshing motion across the width can be produced by rocking the resonator or with the help of a hand-held paddle. This can be very effective if it is done when the drive is first turned on.

Since the frequency of the wave is half that of the drive, the phase of the drive is repeated every 180° of the wave. Consequently solitons which are 0° or 180° apart in phase are compatible and equally driven. Solitons which are 180° out of phase can be generated by sharply twisting the trough about a central vertical axis, so that the sloshing in the left half has the opposite direction of that in the right half. Alternatively an inverted $T$-shaped paddle immersed in the water can be twisted to achieve the same result.

Solitons can be moved in various ways. We have already mentioned tilting the trough. They move in response to gentle jets of air. They can also be nudged by rods of soft sponge plastic. Unwanted

solitons are killed by stabbing them with such rods.

The dashed lines of Fig. 3 describe the range of drive amplitude and drive frequency in which individual solitons are observed without hysteresis. The eight full-line curves are equal–wave-response curves. The number on each is the peak height in centimeters of the soliton above the equilibrium level of the water. Note that at 0.7 and 2.1 cm the curves are so short that they are only represented by points. Outside the dashed boundary, changes in drive amplitude and/or frequency are generally hysteretic. If it exists, the soliton may be unstable, there may be appreciable $x$-dependent phase shifts, and there may be a mixture of modes. At a drive amplitude exceeding 0.081 cm (peak to peak), characteristically a competing mode rather than a soliton appears.

As pointed out earlier, we can generate more than a single soliton in the resonator with the same or opposite polarity. We want now to describe the interaction of two such solitons. Two solitons of the same polarity attract each other, but only weakly if the distance between them is significantly larger (say a factor of 3) than their effective length. Two solitons which start out 20 cm apart center to center, for example, take about 15 min to reach a separation where they strongly overlap. When this happens their attractive speed greatly increases.

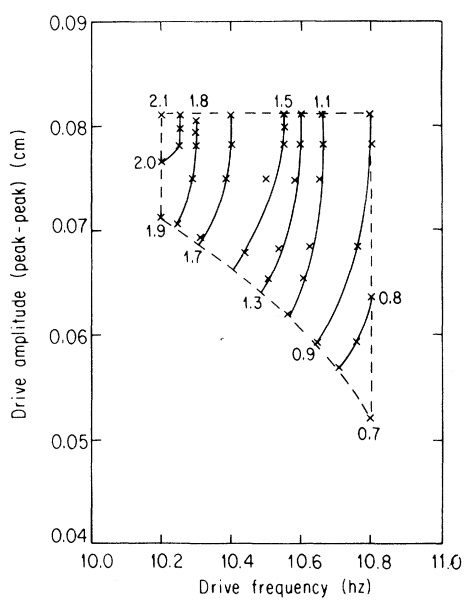


FIG. 3. The range of drive amplitude and drive frequency in which individual solitons are observed without hysteresis. The dashed lines are the boundaries of this region. The eight full-line curves are equal–wave-response curves. The number associated with each curve is the peak height in centimeters of the solitons above the equilibrium level of the water.

If the frequency is substantially lower than the small amplitude $\nu_{0,1}$, the two solitons combine; the end result is a single soliton having the amplitude of each of the initial solitons. If the frequency is closer to the small amplitude $\nu_{0,1}$, the solitons oscillate about each other. Figure 4 is a schematic of the stages of oscillation. In the first stage, 4(a), there is significant overlap. In Fig. 4(b) the overlap is sufficient to create an amplitude at the center which is comparable with the amplitudes of solitons 1 and 2. In Fig. 4(c) the solitons completely overlap. In Fig. 4(d) apparently solitons 1 and 2 have passed through each other and exchanged places while in Fig. 4(e) the configuration is the original one. Left undisturbed this sequence repeats indefinitely. We have observed it for periods of more than an hour. We have never seen the oscillation interrupted except by accident or design.

A simple transducer which responds to wave heights is a pair of vertical wire electrodes that dip into the water. At a constant-voltage drive (ac or dc) the current due to the conductance of the water is proportional to the wave height at the electrodes. Figure 5 shows the response of such a transducer placed at the midpoint of the oscillating solitons of Fig. 4. In the lowest trace, which covers the complete sequence of Fig. 4, the paper speed was great enough so that the individual oscillations are seen ($\nu = 5.32$ Hz). The frequency of the envelope, which is much deeper than the drive, is $2\nu/$

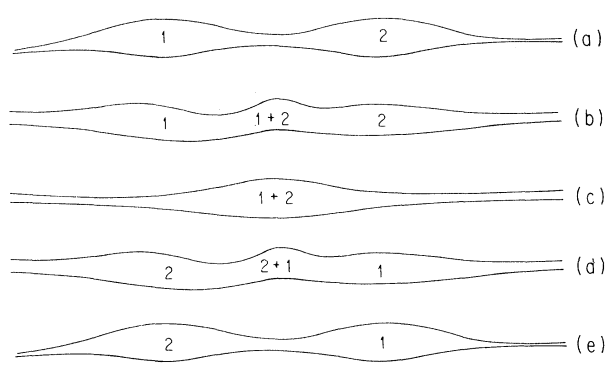


FIG. 4. A schematic of stages in the resulting oscillation of two like-phase solitons. (a) Significant overlap between soliton 1 and soliton 2. (b) Sufficient overlap to create an amplitude at the center comparable to the amplitude of solitons 1 and 2. (c) The solitons completely overlap. (d) Solitons 1 and 2 have passed through each other and exchanged places. (e) The original configuration. Solitons 1 and 2 have exchanged places.

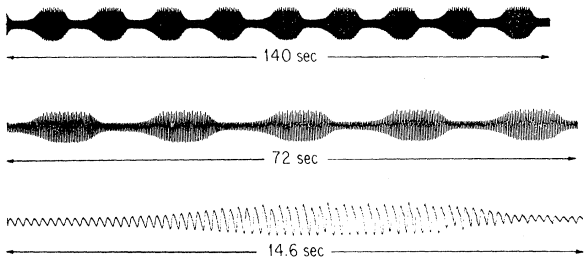


FIG. 5. The response of a height transducer placed at the midpoint of the oscillating solitons of Fig. 4. The lowest trace covers the complete sequence of Fig. 4. The frequency of the envelope is $2\nu/(156 \pm 0.5) = 0.068$ Hz. The upper traces are recorded at successively slower paper speeds.

$(156 \pm 0.5) = 0.068$ Hz. The upper traces are recorded at successively slower paper speeds.

A pair of solitons of opposite polarity in close proximity to each other repel each other and slowly move until they are approximately 12 cm apart, and then maintain this separation indefinitely. Again we have never seen this state to be interrupted except by accident or design. We understand the attraction and repulsion of solitons in terms of the Bernoulli effect. In the overlap region the particle velocity increases for the like pair and decreases for the unlike pair, decreasing or increasing, respectively, the pressure between them.

By introducing tracers (eccospheres) into the water we have been able to establish that the motion of solitons is one in which there is a transport of excitation with negligible transport of mass.

We wish to acknowledge informative conversations with John Miles, Joseph Rudnick, and L. A. Turkevich. We especially benefitted from interaction with Andres Larraza and Seth Putterman who will shortly submit for publication a paper on the theory of such a soliton. This work was supported in part by the U. S. Office of Naval Research.

[1]Lord Rayleigh, *The Theory of Sound* (Dover, New York, 1945), Sec. 68b.

[2]T. B. Benjamin and F. Ursell, Proc. Roy. Soc. London, Ser. A **225**, 505 (1954); R. Keolian, L. A. Turkevich, S. J. Putterman, I. Rudnick, Phys. Rev. Lett. **47**, 1133 (1981).

[3]L. D. Landau and E. M. Lifshitz, *Fluid Mechanics* (Pergamon, London, 1959).

[4]L. E. Kinsler, A. R. Frey, A. B. Coppens, and J. V. Sanders, *Fundamentals of Acoustics* (Wiley, New York, 1982), pp. 216–222. Here waveguide theory for sound is discussed.

[5]A. C. Scott, F. Y. F. Chu, and D. W. McLaughlin, Proc. IEEE **61**, 10 (1973).